A 3D Monte Carlo Code for Plasma Transport in Island Divertors

Y. Feng, F. Sardei, J. Kisslinger, P. Grigull

IPPIII/208

December 1996

MAX-PLANCK-INSTITUT FÜR PLASMAPHYSIK

85748 GARCHING BEI MÜNCHEN

MAX-PLANCK-INSTITUT FÜR PLASMAPHYSIK

GARCHING BEI MÜNCHEN

A 3D Monte Carlo Code for Plasma Transport in Island Divertors

Y. Feng, F. Sardei, J. Kisslinger, P. Grigull

IPPIII/208

December 1996

Die nachstehende Arbeit wurde im Rahmen des Vertrages zwischen dem Max-Planck-Institut für Plasmaphysik und der Europäischen Atomgemeinschaft über die Zusammenarbeit auf dem Gebiete der Plasmaphysik durchgeführt.

A 3D Monte Carlo Code for Plasma Transport in Island Divertors

Y. Feng, F. Sardei, J. Kisslinger, P. Grigull

Max-Planck-Institut für Plasmaphysik, EURATOM Ass.,

D-85748 Garching, Germany

Abstract

A fully 3D self-consistent Monte Carlo code EMC3 (***Edge Monte Carlo 3D***) for modelling the plasma transport in island divertors has been developed. In a first step, the code solves a simplified version of the 3D time-independent plasma fluid equations. Coupled to the neutral transport code EIRENE, the EMC3 code has been used to study the particle, energy and neutral transport in W7-AS island divertor configurations. First results are compared with data from different diagnostics (Langmuir probes, H_α cameras and thermography).

1. Introduction

Unlike in tokamaks, the magnetic structure and the discontinuous target plates in the W7-AS and W7-X stellarators introduce a three-dimensional plasma boundary. This implies that, for high recycling conditions, 3D effects of plasma, neutral and impurity transport have to be taken into account by both transport modelling and diagnostics [1]. In this paper, a fully 3D self-consistent Monte Carlo code EMC3 is presented, which solves, in a first step, a simplified version of the 3D time-independent fluid equations for plasma transport in island divertors. The main assumptions are $T_i=T_e$ (i.e. strong ion/electron collisional coupling), neglect of heat convection and parametrization of momentum losses due to viscosity and CX with neutrals. The particle, momentum and energy balance equations are solved iteratively in sequence. All diffusive terms are treated by following Monte Carlo particles in 3D magnetic coordinates. Particle diffusivity is assumed to be anomalous and the transport coefficients are taken from the

experiment. Energy transport is considered to be dominated by classical parallel and anomalous cross-field heat conduction. Islands, private flux region and targets plates are modelled in their real 3D geometry. High flexibility is provided by EMC3 to locally adjust the grid according to the required resolution, for example, finer grid near to the targets. Coupled to the neutral transport code EIRENE [2], the EMC3 code has been used to investigate the particle, energy and neutral transport in W7AS island divertor configurations.

The code has been first applied to the proposed island divertor of W7-AS, for which it predicts high recycling conditions associated with a strong density rise inside the islands. The results have motivated intensive experimental studies in order to clarify whether the predicted island high recycling can be obtained with the present inboard target plates. Simulations will be compared to data from different diagnostics.

2. Simplified one-fluid model

Although the transports of charged particles are best described by kinetic theory, solving the full kinetic equations remains an infeasible task. Instead, the edge plasma is commonly treated as a multi-fluid [3]. In the first step towards a full solution of the 3D Navier-Stokes equations, we assume a simple neutral plasma consisting of electrons and a single ion species. The plasma is considered to be dense enough that thermal equilibrium holds between electrons and ions, $T_i=T_e=T$. Parallel and perpendicular heat conductions are considered to dominate the energy transport. With a parametrization of the momentum losses due to viscosity and neutrals, the balance equations for mass, momentum and energy are given by

$$\nabla\cdot(n\mathbf{v}_{\parallel} - D_{\perp}\nabla_{\perp}n) = S_p \qquad (2.1)$$

$$\nabla_{\parallel}(m_i n v_{\parallel}^2 + p) = -\alpha_m \qquad (2.2)$$

$$\nabla\cdot(-\kappa_{\parallel}\nabla_{\parallel} T - \chi_{\perp} n \nabla_{\perp} T) = S_e \qquad (2.3)$$

with the Bohm conditions for the particle flux Γ_t and the heat flux q_t at the target

$$\Gamma_t = n\, C_t \qquad (2.4)$$

$$q_t = \gamma T \Gamma_t \qquad (2.5)$$

where p is the plasma pressure, S_p and S_e are the volume sources of particle and energy determined by the EIRENE code and α_m is a constant momentum loss parameter determined by upstream and downstream measurements. The parallel heat conduction is considered to be classical, while the cross-field particle diffusion and heat conduction are assumed to be anomalous with $D_\perp$ and $\chi_\perp$ being determined from experiments. Particles are lost to the target plates at sound speed C_t with energy γT where γ is the energy transmission coefficient at the sheath. Plasma density and heat flux are given as boundary conditions at the separatrix.

3. Monte Carlo method

Due to the complicated geometry related to the island chain and the discontinuous target plates, the construction of a locally optimized grid for a finite difference solver may become problematic. This is not the case for the Monte Carlo method because of its high flexibility in the grid mesh construction and distribution . The grid can be locally adjusted according to the required resolution. The energy and particle transport equations are treated by the Monte Carlo method, whereas the momentum balance equation is solved analytically, as will be discussed later.

3.1 Particle transport

The particle transport equation (2.1) can be rewritten in the following time-independent Fokker-Planck form

$$\nabla_{\parallel}\cdot(-\mathbf{v}_{\parallel} n) + \nabla_{\perp}\cdot[\nabla_{\perp}(D_{\perp}n) - n\nabla_{\perp}D_{\perp}] + S_p = 0. \qquad (3.1)$$

Equation (3.1) describes the density distribution of particles diffusing across B with the mean convection velocity $\mathbf{v}_{\parallel}$. It can be solved by a random walk procedure [4]. Particles are randomly generated according to a volume or a surface source distribution on the LCFS, and then followed in small time steps Δt. The particle walks a step $\Delta \mathbf{r}$ given by

$$\Delta \mathbf{r} = (4D_{\perp}\Delta t)^{1/2}\,\xi_{\perp} + \nabla_{\perp}D_{\perp}\Delta t + \mathbf{v}_{\parallel}\Delta t \qquad (3.2)$$

where $\xi_\perp$ is the random unit vector perpendicular to B. Equation (3.2) indicates that the magnetic field line vector is required for tracing particles in two different directions. In order to avoid repeating the calculations of the magnetic field lines, it is convenient to trace particles in magnetic coordinates (r^m,θ^m,ϕ^m), where the field line is a straight line with pitch $\Delta\theta^m/\Delta\phi^m=\iota$. Particles are traced and scored in the given grid mesh. If a particle is lost to a target plate, a new particle is generated and the computation continues until the desired accuracy of statistic is obtained.

In order to speed up the computation, it is necessary to represent the target plates in magnetic coordinates as well.

3.2 Momentum balance

In the absence of perpendicular coupling, the momentum balance equation (2.2) can be integrated immediately. Assuming that $v_\parallel$ reaches the sound speed at the target plate, we have simply

$$m_i n v_\parallel^2 + p = 2p_t - \alpha_m l_\parallel \qquad (3.3)$$

where p_t and $l_\parallel$ are the thermal pressure at the target and the parallel distance from the target, respectively. Since the kinetic pressure, except in the region close to target plates, is a small quantity as compared to the thermal pressure, $v_\parallel$ can hardly be deduced directly from the equation (3.3) due to the statistical errors in p resulting from the Monte Carlo method. Instead, we treat the problem in an indirect way. Note that p=2nT and T remain unchanged during the iterative determination of n and $v_\parallel$. From equation (3.3) we get

$$n_m=(2p_t - \alpha_m\ l_\parallel\ )/(m_i v_\parallel^2 + 2T) \qquad (3.4)$$

where the subscript m on the density n is introduced in order to distinguish it from n as determined by the particle transport equation. Equation (3.4) gives a density distribution

required to satisfy the momentum balance. Comparing n_m with n and taking into account the fact that $n \propto 1/v_{||}$, we get $v_{||new}$ for the next iteration

$$v_{||new} = (m_i n v_{||}^2 + 2nT)/(2p_t - \alpha_m l_{||}) \cdot v_{||} . \quad (3.5)$$

As seen from (3.5), $v_{||}$ at the target plate remains unchanged. Therefore, an initial distribution for $v_{||}$ satisfying the boundary condition $v_{||t}$=sound speed at both target plates is required. This can be easily provided by assuming two groups of particles streaming initially antiparallel to each other. After replacing $v_{||}$ in the particle transport equation (3.1) by $v_{||new}$, the iteration starts and continues until n and $v_{||}$ converge.

3.3 Energy transport

With the definitions of $E=<n>T$, $n_x=n/<n>$ and $\kappa_{||x}=\kappa_{||}/<n>$, where <n> is the average density at the separatrix, the energy transport equation (2.3) can be rewritten as

$$\nabla_{||}\cdot[\nabla_{||}(\kappa_{||x}E) - E\nabla_{||}\kappa_{||x}] + \nabla_{\perp}\cdot[\nabla_{\perp}(n_x\chi_{\perp}E) - E\nabla_{\perp}(n_x\chi_{\perp})] + S_e = 0 \quad (3.6)$$

where S_e in the present version of the code, is the volume energy loss or gain due only to the hydrogen neutrals. The equation (3.6) is of the same form as the particle transport equation (3.1). Therefore, the procedure applied for the particle transport can be used for solving the equation (3.6). Now the Monte Carlo particles represent heat quantities. A subiteration process is required in this case, as the classical heat conductivity depends strongly on the temperature ($\kappa_{||} \propto T^{5/2}$).

3.4 Solution sequence

The computation starts with the energy transport, which is very sensitive to the temperature distribution. Particles representing heat quantities are randomly generated on the LCFS and followed initially in a source-free background plasma of constant density and temperature. The temperature distribution is then determined by iteration. Then, the neutral transport code EIRENE is called to provide the volume sources for the plasma. Particles started according to

S_p from the EIRENE code are initially divided into two groups streaming antiparallel to each other in order to satisfy the sound speed boundary condition at both target plates. $v_{||}$ is then corrected according to the momentum balance equation. Finally, n and $v_{||}$ are determined by sequential iteration of the particle transport and momentum balance equations. This step completes the sequence of the main iteration loop. After inserting n and S_e into the energy transport equation, the main and subiterations continue until T, n and $v_{||}$ converge.

4. Applications

The code was first applied to the proposed island divertor configuration of W7AS (**Fig.1**). The ι =5/9 island chain is intersected by ten up/down symmetric target plates extending 18° toroidally. First results show a strong dependence of the ratio of parallel to perpendicular transport fluxes on the connection lengths governed by the island rotational transform ι_i [5]. It can be varied by changing the ratio modular/toroidal field currents and the current of the control coils. ι_i has to be sufficiently large to overcome the perpendicular transport across the islands, but sufficiently small to provide a sufficient radial power flow to allow ionization of the neutrals in the island core. For $\iota_i \approx 0.1$, **Figure 2** shows the density profiles across the island for three density values at the LCFS with the same heat flux through the separatrix (q=0.5 MW). Neither viscosity nor momentum loss via neutrals are taken into account (α_m=0). In the high density case, the simulations predict a density rise by a factor two from the LCFS to the island O-point, indicating high recycling inside the islands. The high density in the island can partially compensate for the relatively small radial distance from the target plates to the main plasma. The temperature profiles for the three cases, on the other hand, do not significantly differ from each other, as the parallel heat conduction dominates the energy transport (**Fig.3**). Neutrals are ionized by more than 90% outside the LCFS and well confined by the baffles (**Fig.4**).

Recently, island divertor experiments at ι_a=5/9 have been performed in W7AS with the islands intersected by 10 symmetric inboard target plates, aimed to explore the high recycling

conditions predicted by the theory. In this case, the simulations are concentrated on the density dependence of the recycling behaviour, focussing on the effort to explain the experimental observations.

Simulations are made for four NBI discharge series, covering a range of line-averaged density $\langle n_e \rangle_{line}$ between $2*10^{19}$ and $1.2*10^{20}$ m^{-3}. The heat fluxes across the inner separatrix are 0.4 MW for $\langle n_e \rangle_{line} = 2*10^{19}$, $4*10^{19}$ and $8*10^{19}$ m^{-3}, and 0.9 MW for the highest density, and are estimated from the NBI power deposition and core radiation. Additional power losses in the SOL are considered due only to the neutrals. The pressure drop factor α_m is estimated from the upstream and downstream measurements of two Langmuir probes [6]. The cross-field diffusion coefficient $D_\perp$ and the density at the inner separatrix $n_{e\text{-}sep}$ are determined by the Langmuir probe profile data across an island, and adjusted in such a way as to match the measured profiles [6]. The results for the four density values are summarized in **figure 5**. The measured density profiles are rather flat except for the highest $\langle n_e \rangle_{line}$, for which the density peaks close to the outer separatrix. In all the cases the profiles are well reproduced by the code. For $\langle n_e \rangle_{line} \leq 8*10^{19}$ m^{-3}, the resulting diffusion coefficient $D_\perp$ is 0.6 m^2/s, dropping to 0.2 m^2/s as the density increases to $1.2*10^{20}$ m^{-3}. $\chi_\perp$ is assumed to be $3D_\perp$ for all the cases. The corresponding measured and simulated temperature profiles for the highest and lowest $\langle n_e \rangle_{line}$ are shown in **figure 6**. The higher temperature predicted for the highest denstiy is probably due to the missing impurity radiations in the code. **Figure 7** shows the $H\alpha$ and the flux amplication factor, as well as the downstream densities and temperatures for the same discharges as functions of $\langle n_e \rangle_{line}$. At relatively low densities ($\langle n_e \rangle_{line} \leq 8*10^{19}$ m^{-3}), the downstream density and $H\alpha$ show a linear dependence on $\langle n_e \rangle_{line}$. At the highest density, the abrupt steepening of the downstream density, of the flux amplification factor and of the measured and calculated $H\alpha$ gives evidence of high recycling. Temperatures near the plates decrease with increasing density, but remain sufficiently high to allow ionizations of the neutrals in the island. The 2D distribution of density and temperature in the inboard target cross section, obtained from the EMC3/EIRENE code for the high recycling case, is shown in

figure 8. Strong pressure drop is experimentally found along the island fans, even for the low density cases in which the neutrals could not make significant contributions. This is probably due to the enhanced $\perp$ anomalous viscosity related to the special island geometry in W7AS. The island fans represent two close channels of antiparallel particle flows to the targets. Momentum loss occurs if particles in the two channels exchange their momentum by means of cross-field diffusion. This effect may be very pronounced in W7AS because of the small size of the islands.

Despite the small field line pitch in the island ($\iota_i \approx 0.1$), the parallel heat conduction dominates the energy transport, which has been confirmed both by the thermography and the simulations. **Figure 9** shows the energy flux distribution on a target plate resulting from EMC3 together with the surface temperature distribution from thermography. Both show a strong localization of the energy flux along the island fan with the largest connection length. In contrast to the energy flow which is governed by the island diversion, the particle flux depends more on the recycling conditions and the neutral flows. **Figure 10** shows vertical scans of H_α data from the diode array looking at the target and from the code. Both indicate that the recycling peaks at the outermost strike points. Simulations show that more than 60% of particles intersect the targets on the side, leading to a poloidally wide spread of the neutrals.

5. Conclusions

A 3D self-consistent Monte Carlo code EMC3 has been developed, aimed at investigating the edge transport in stellarators in the presence of islands. At present, the code solves a simplified version of the 3D time-independent plasma fluid equations. The code provides a high flexibility in the grid construction, so that it can be easily adapted to any complicated 3D edge topology of stellarators. Coupled to EIRENE, the EMC3 code simulates self-consistently the plasma and neutral transport in a full 3D space. Alternatively, the code can be used as a fit procedure to estimate the transport parameters by matching the local experimental data. In a first application

to the proposed divertor configuration in W7-AS, the code predicts a density rise consistent with high recycling conditions in the islands. Similar behaviour has been observed experimentally in W7-AS with the inboard target configuration. The code results are supported by different diagnostics (Langmuir probes, H_α diode array and thermography).

6. References

[1] F. Sardei, et al., *Island divertor studies on W7-AS*. 12th int. Conf. on Plasma Surface interaction, Saint Raphael, France, 1996, accepted for publication in J. Nucl. Materials

[2] D. Reiter, J. Nucl. Mat. 196-198 (1992) 80

[3] B.J. Braams, Ph.D. Thesis, Rijksuniversiteit Utrecht (1986)

[4] Van Kampen, N.G., "Stochastic Processes in Physics and Chemistry", North-Holland Publishing Company, Amsterdam - New York - Oxford, 1981

[5] Y. Feng, et al., 22th EPS Conf. on Contr. Fusion and Plasma Physics, Bournemouth 1995, ECA 19C,IV,325

[6] P. Grigull, et al., *Experimental study on high collisional edge plasmas in W7-AS island divertor configurations*, 12th int. Conf. on Plasma Surface interaction, Saint Raphael, France, 1996, accepted for publication in J. Nucl. Materials

Fig. 1: Arrangement of the proposed divertor for W7-AS.

Fig. 2: *Left:* Density profiles across the island, averaged over the toroidal range of the plate. The three curves correspond to three densities at the LCFS: $5*10^{18}$ (dashed), $1*10^{19}$ (dot-dashed) and $2*10^{19}$ (solid) m^{-3}. *Right:* 2D distribution of density in the elliptical cross section for the high recycling case.

Fig. 3: Temperature profiles across the island, averaged over the toroidal range of the plate. The three curves correspond to three densities at the LCFS: $5*10^{18}$ (dashed), $1*10^{19}$ (dot-dashed) and $2*10^{19}$ (solid) m^{-3}.

Fig. 4: 2D distribution of atom density in the elliptical cross section for the high recycling case.

Fig. 5: Measured and calculated density profiles across an island.

Fig. 6: Measured and calculated temperature profiles for the highest and lowest line-averaged densities.

Fig. 7: Downstream densities and temperatures (top), flux amplification factor and H_α (bottom) from measurements and simulations versus the line-averaged denstity.

Fig. 8: 2D distribution of the calculated density (left) and temperature (right) in the inboard target cross section for the highest line-averaged density.

Fig. 9: *Top:* Surface temperature distribution on a target plate from thermography (left) and the distribution of the heat flux from the EMC3 code (right). *Bottom:* Heat flux distribution on the lowest segment of an inboard plate from the thermography and the EMC3 code.

Fig.10: Vertical scans of H_α data (left) from the diode array and from the EMC3/EIRENE code together with the 2D distribution of atom density (right).

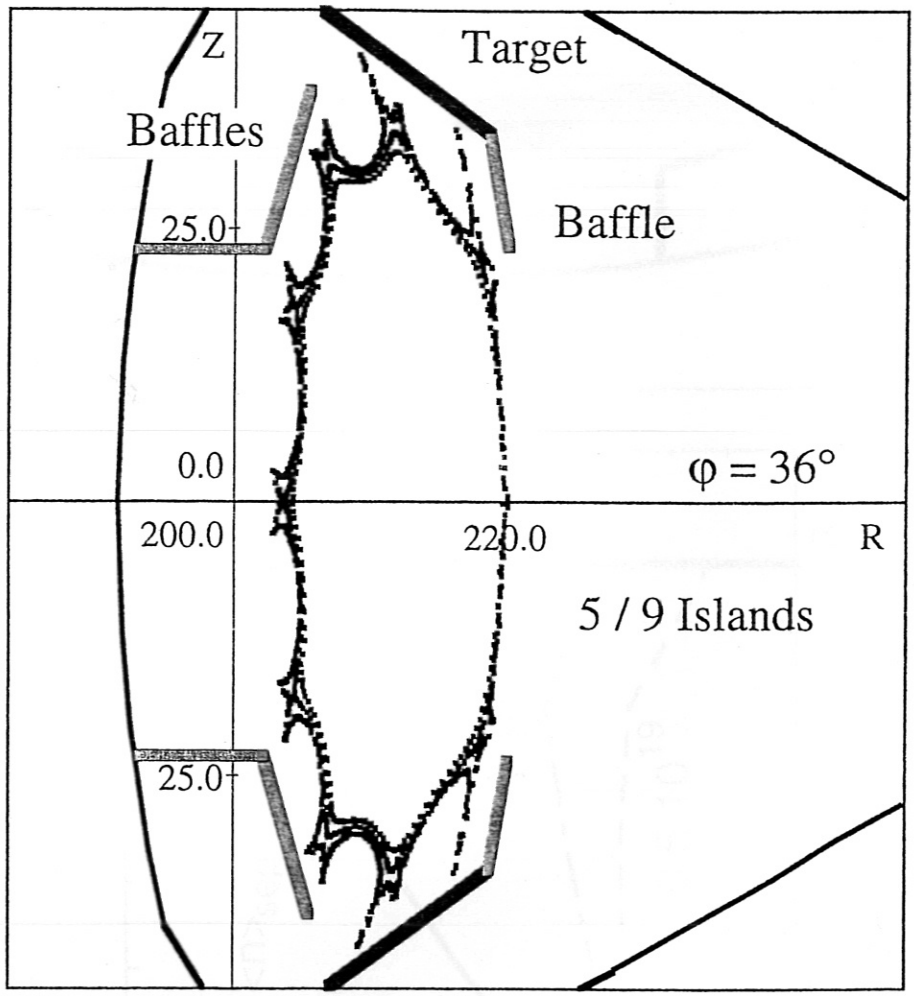

Fig. 1

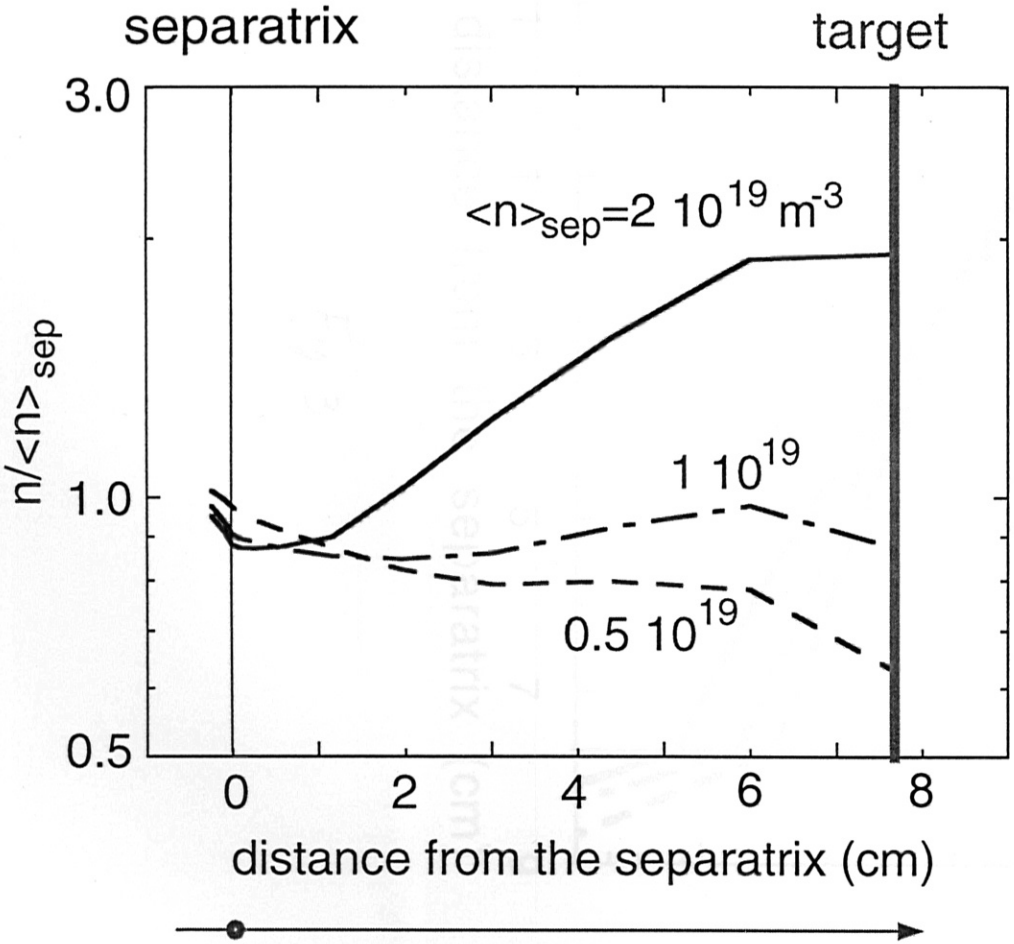
separatrix
target
3.0
1.0
0.5
n/<n>sep
<n>sep=2 10^19 m^-3
1 10^19
0.5 10^19
0
2
4
6
8
distance from the separatrix (cm)

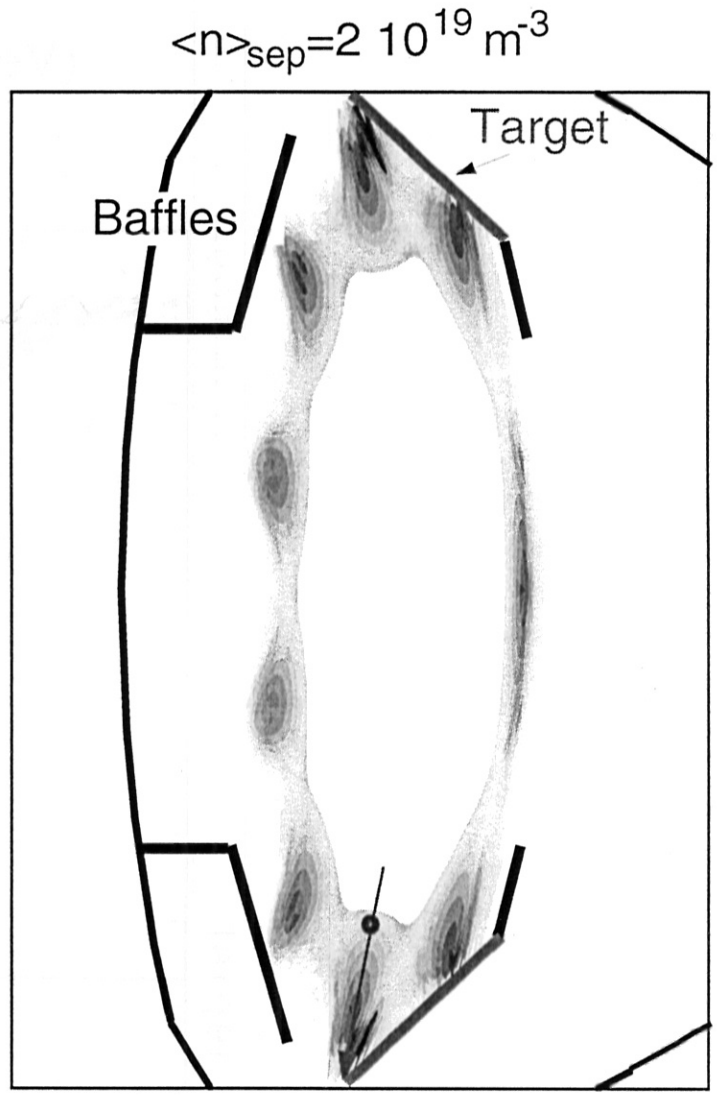
<n>sep=2 10^19 m^-3
Target
Baffles

Fig 2

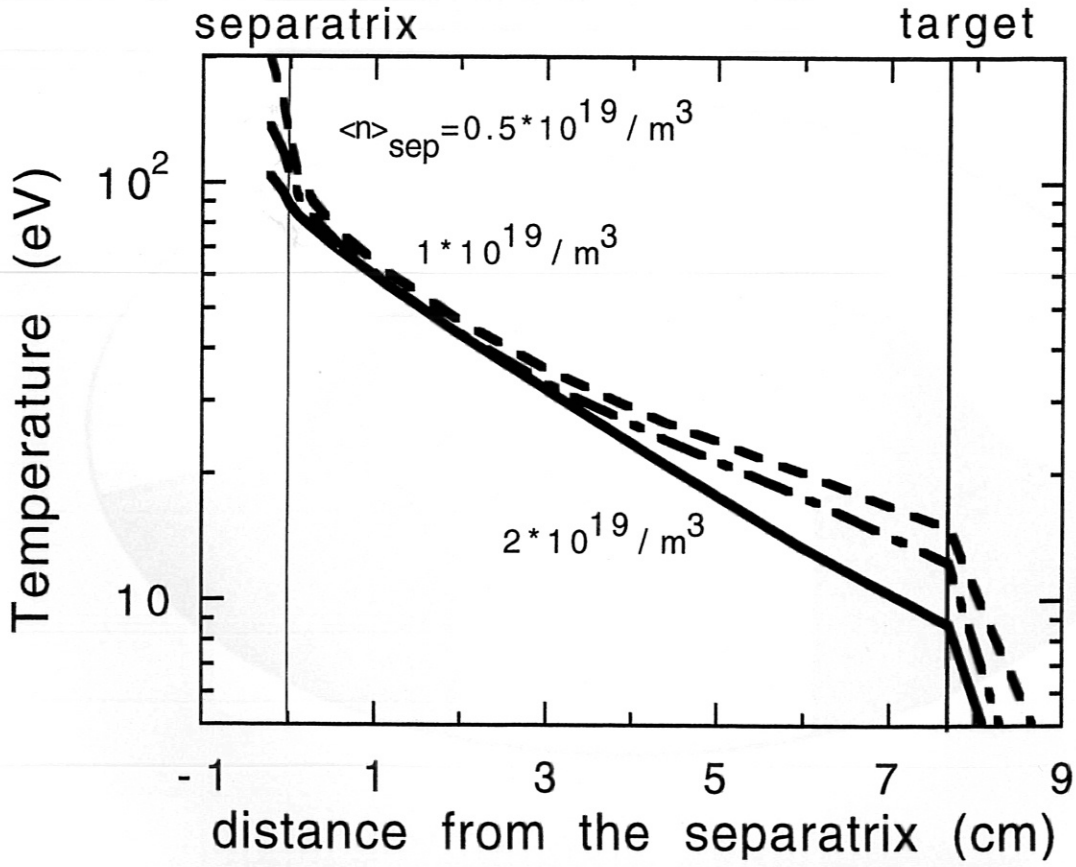
separatrix
target
<n>sep=0.5*10^19 / m^3
1*10^19 / m^3
2*10^19 / m^3
Temperature (eV)
10^2
10
-1
1
3
5
7
9
distance from the separatrix (cm)

Fig 3

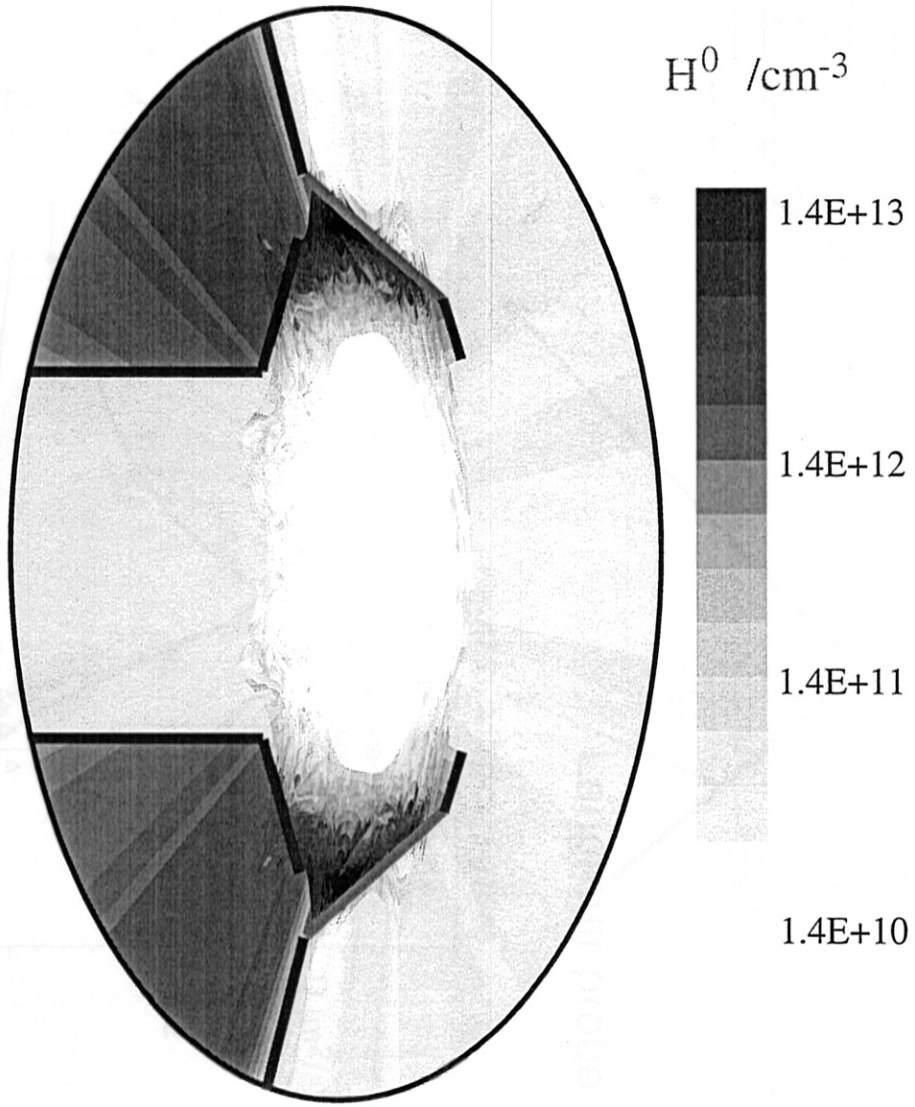

Fig. 4

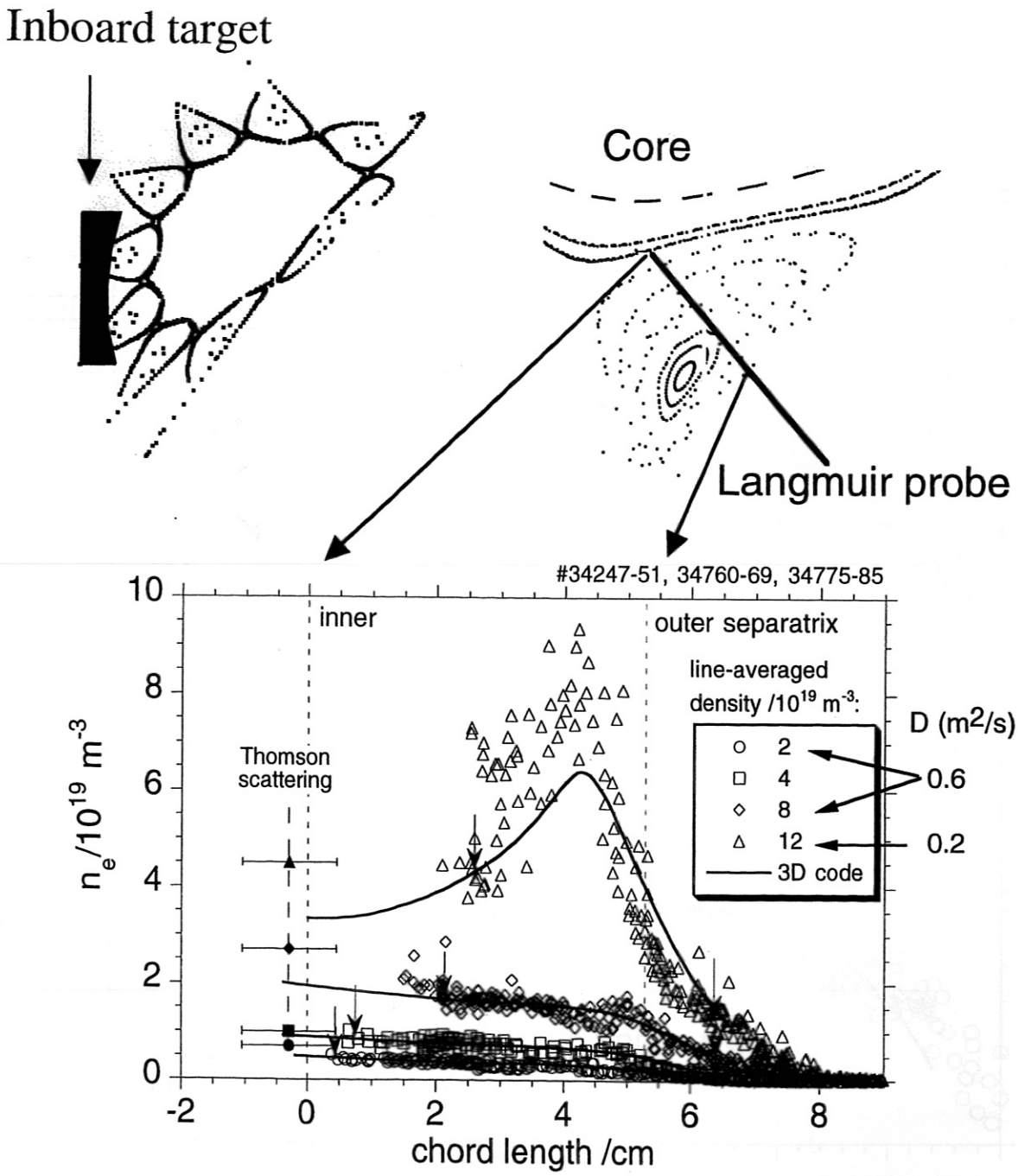
Inboard target
Core
Langmuir probe
#34247-51, 34760-69, 34775-85
inner
outer separatrix
line-averaged
density /10^19 m^-3:
2
4
8
12
3D code
D (m^2/s)
0.6
0.2
Thomson
scattering
n_e/10^19 m^-3
chord length /cm

Fig. 5

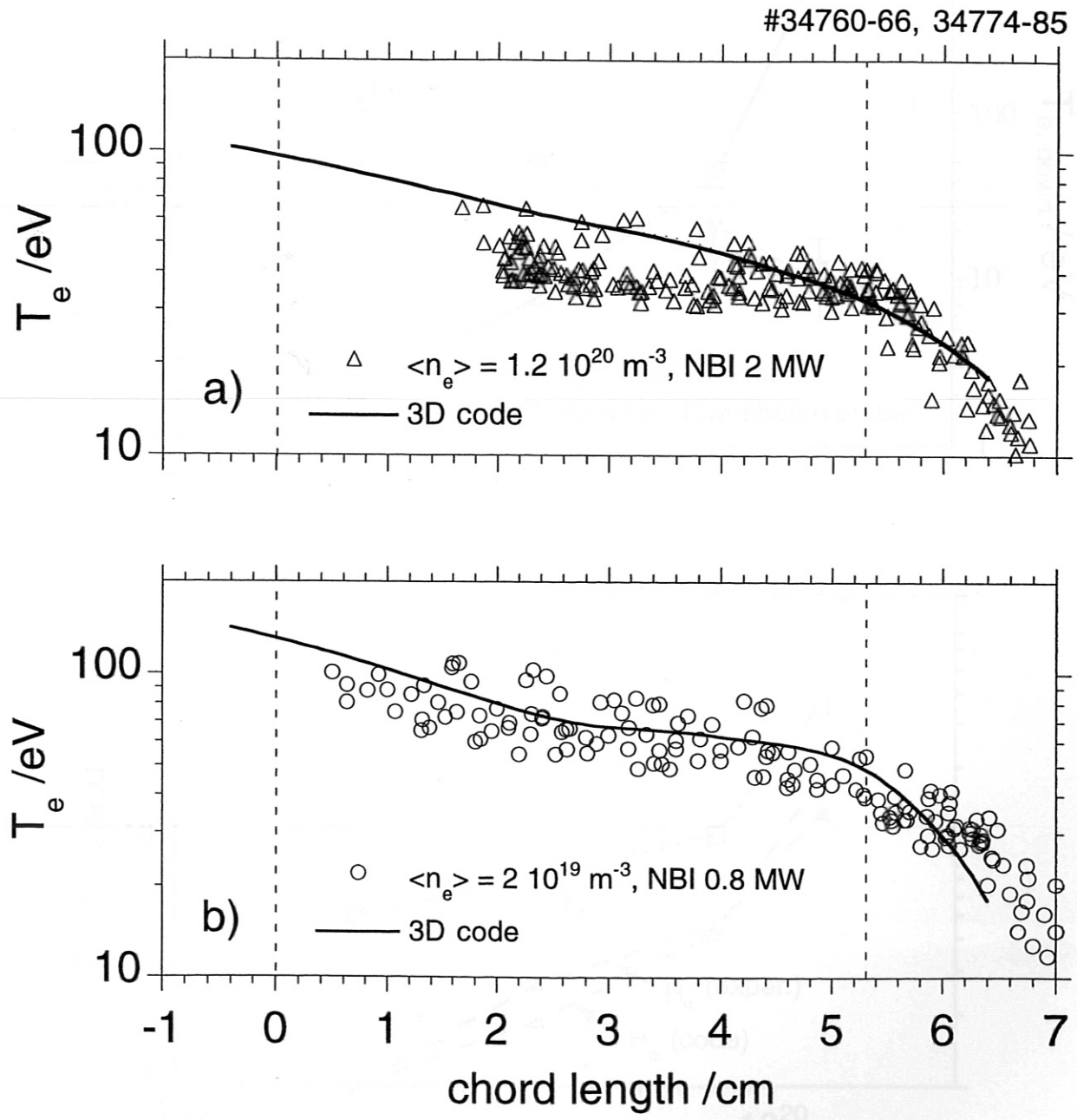
#34760-66, 34774-85
100
10
T_e /eV
a)
$\langle n_e \rangle$ = 1.2 10^{20} m^{-3}, NBI 2 MW
3D code
b)
$\langle n_e \rangle$ = 2 10^{19} m^{-3}, NBI 0.8 MW
3D code
-1
0
1
2
3
4
5
6
7
chord length /cm

Fig. 6

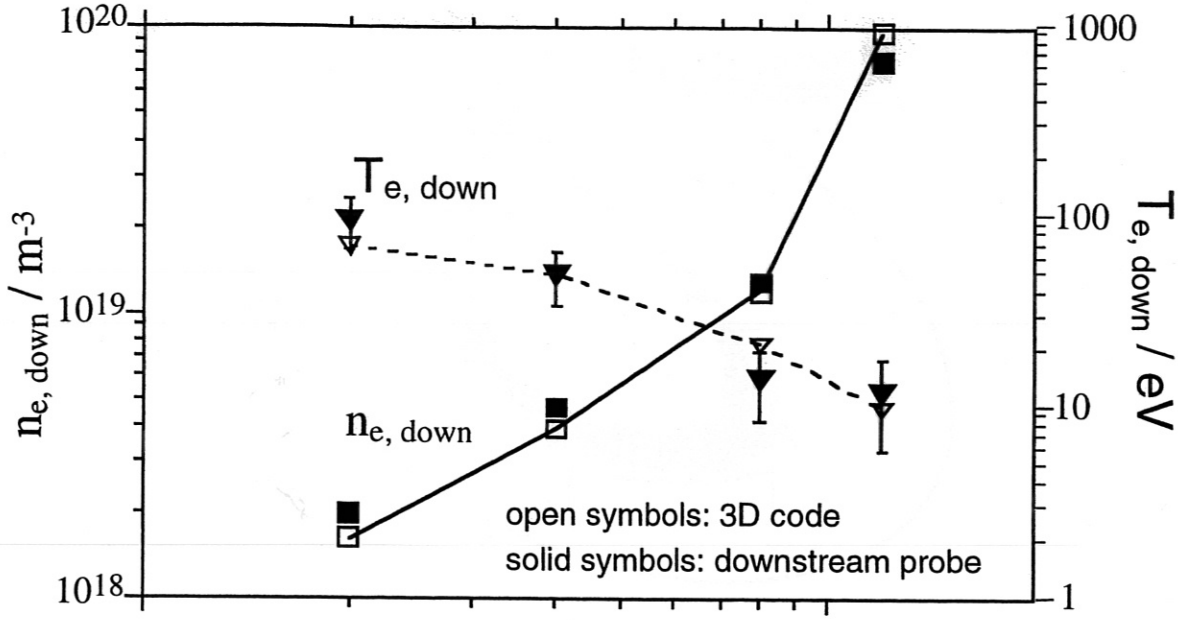
10^{20}
10^{19}
10^{18}
$n_{e,\,down}$ / m^{-3}
1000
100
10
1
$T_{e,\,down}$ / eV
$T_{e,\,down}$
$n_{e,\,down}$
open symbols: 3D code
solid symbols: downstream probe

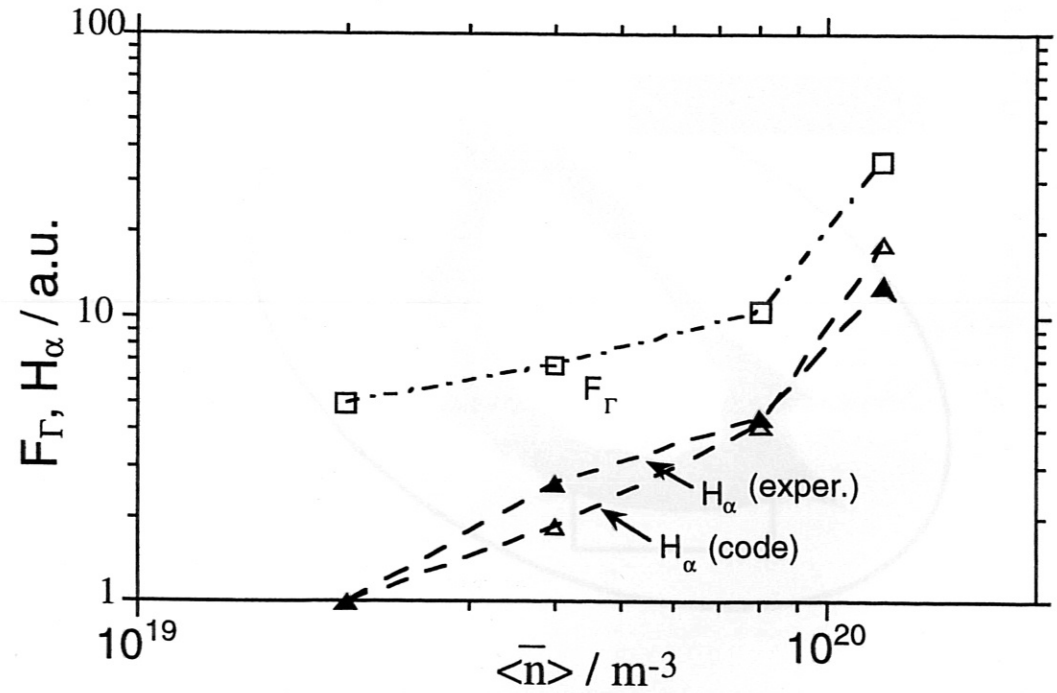
100
10
1
F_Γ, H_α / a.u.
F_Γ
H_α (exper.)
H_α (code)
10^{19}
10^{20}
$\langle\bar{n}\rangle$ / m^{-3}

Fig. 7

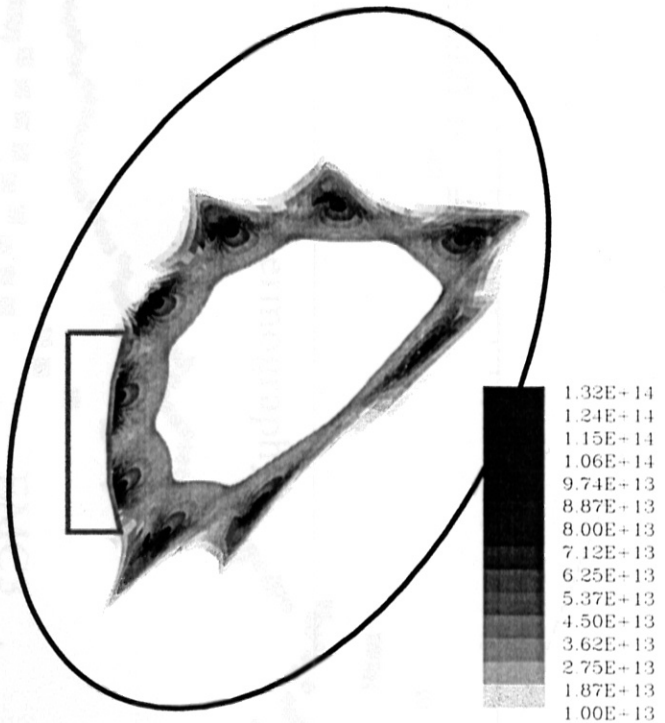
1.32E+14
1.24E+14
1.15E+14
1.06E+14
9.74E+13
8.87E+13
8.00E+13
7.12E+13
6.25E+13
5.37E+13
4.50E+13
3.62E+13
2.75E+13
1.87E+13
1.00E+13
n_e / cm^{-3}

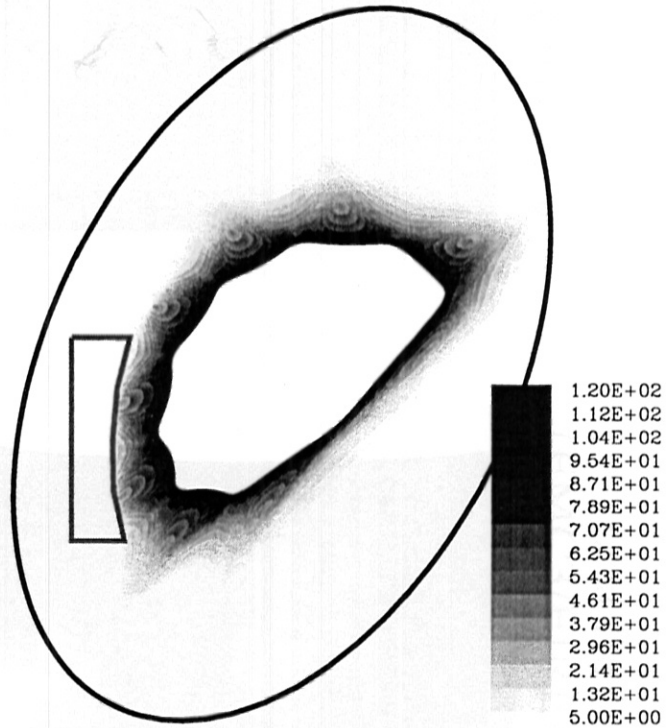
1.20E+02
1.12E+02
1.04E+02
9.54E+01
8.71E+01
7.89E+01
7.07E+01
6.25E+01
5.43E+01
4.61E+01
3.79E+01
2.96E+01
2.14E+01
1.32E+01
5.00E+00
T_e (eV)

Fig. 8

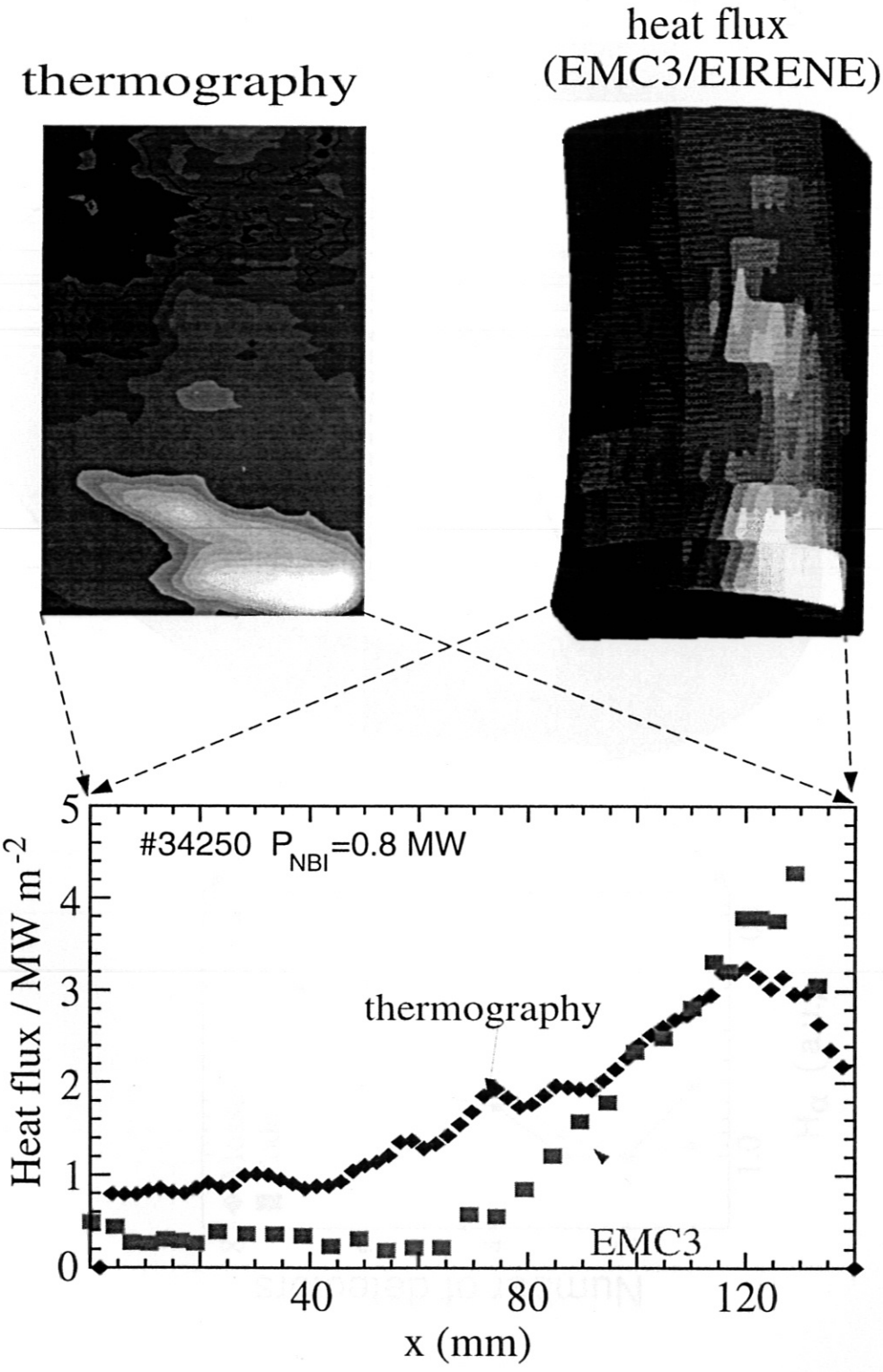
thermography
heat flux
(EMC3/EIRENE)
#34250 P_NBI=0.8 MW
thermography
EMC3
Heat flux / MW m^-2
x (mm)
0
1
2
3
4
5
40
80
120

Fig 9

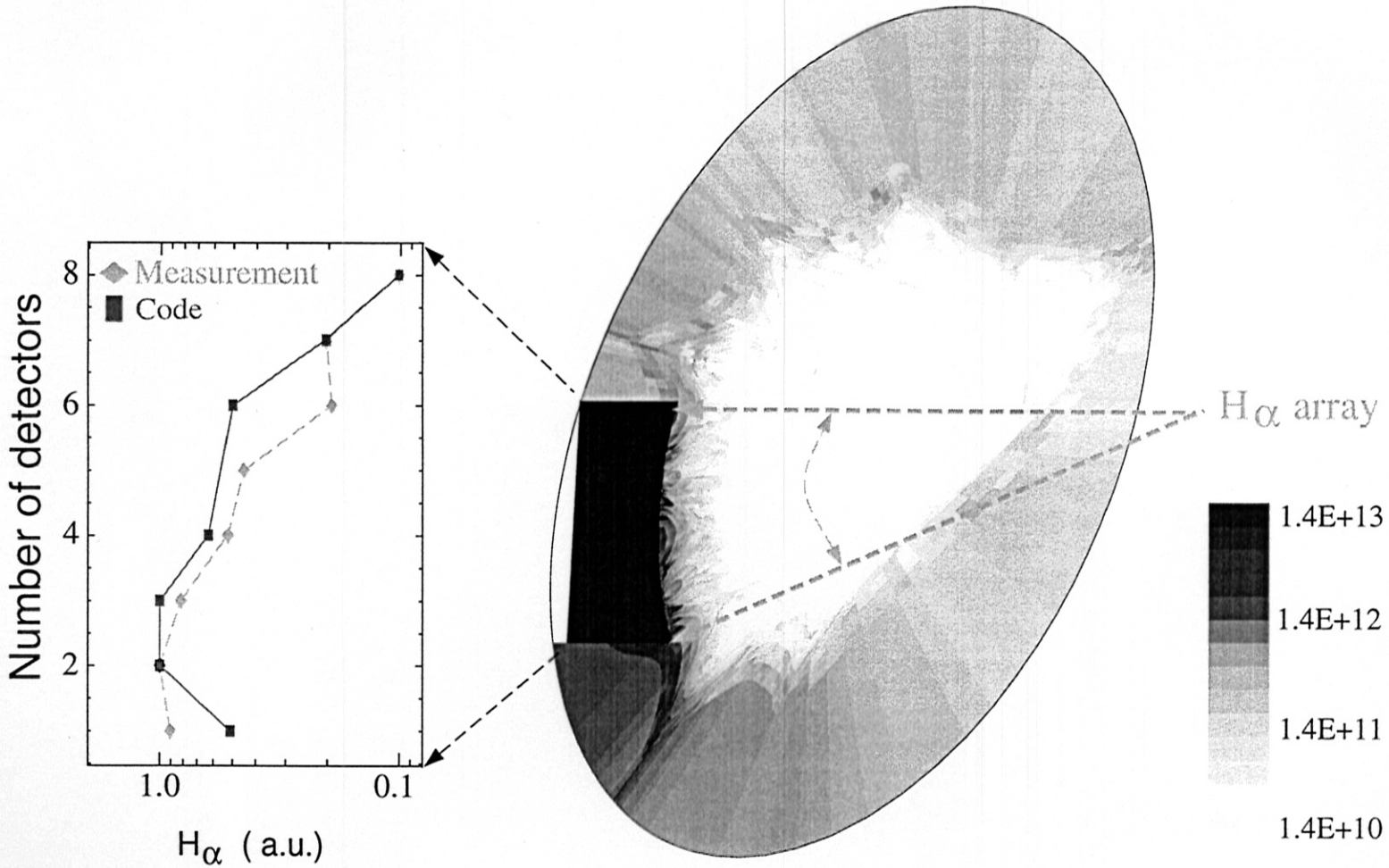
Number of detectors
8
6
4
2
Measurement
Code
1.0
0.1
Hα (a.u.)
Hα array
1.4E+13
1.4E+12
1.4E+11
1.4E+10

Fig 10